

Lattice Calculation of Gluon Screening Masses

A. Nakamura, and T. Saito

*Research Institute for Information Science and Education,
Hiroshima University, Higashi-Hiroshima 739-8521, Japan*

S. Sakai

Faculty of Education, Yamagata University, Yamagata 990-8560, Japan

We study $SU(3)$ gluon electric and magnetic masses at finite temperatures using the quenched lattice QCD on a $20^2 \times 32 \times 6$ lattice. We focus on temperature regions between $T = T_c$ and $6T_c$, which are realized in RHIC and LHC experiments. Stochastic quantization with a gauge-fixing term is employed to calculate gluon propagators. The temperature dependence of the electric mass is found to be consistent with the hard-thermal-loop perturbation, and the magnetic mass has finite values in the temperature region of interest. Both screening masses have little gauge parameter dependence. The behavior of the gluon propagators is very different in the confinement/deconfinement physics. The short distance magnetic part behaves like a confined propagator even in the deconfinement phase. Simulation with larger lattice, $32^2 \times 48 \times 6$, shows that the magnetic mass has a stronger finite size effect than the electric mass.

PACS numbers: 12.38.Mh, 11.10.Wx, 12.38.Gc, 11.15.Ha

Keywords: lattice QCD, gluon, screening, HTL resummation, gauge fixing

I. INTRODUCTION

One of the most interesting features of QCD (quantum chromodynamics) is the transition from the confinement to the deconfinement phase. In this new state of QCD, quarks and gluons confined in the hadron at zero temperature move freely when the system reaches a sufficiently high temperature. QGP (quark gluon plasma) was realized at high temperature in the early universe, and is expected to be produced in heavy-ion collision experiments at SPS, RHIC and LHC. Thus it is an urgent task to accumulate theoretical knowledge about QGP.

The massless gluon in QGP medium is changed into a dressed massive gluon after quantum corrections. The screening effect is characterized by a mass pole of the propagator and is closely related to thermal QCD phenomenology. One example is a screened heavy quark potential, which is frequently discussed with the relation of J/ψ or Υ suppression. For calculations of jet quenching, which might be a finger print of QGP, a model including the electric and magnetic masses has been proposed [1]. The nonperturbative quantitative study in the vicinity of T_c and up to several times T_c , is of great importance for understanding QGP physics.

The thermal field theory [2, 3, 4] is the most basic method of studying QGP and has provided many informative observations. At zero temperature, many calculations based on perturbative QCD have described experiment results [5] and there is no doubt that QCD is a theory of strong interaction. It is natural to employ the perturbative approach to thermal QCD. Due to the asymptotic freedom at high temperature, the coupling constant is expected to become small enough to carry out the perturbations. In such a high energy state, quarks and gluons must behave as an ideal gas; yet this simple consideration is spoiled by an infrared divergence [6], which is known to bear a hierarchy on the energy scale in the QGP system [3, 4]. One usually defines $1/T$ as a perturbative length scale, and furthermore $1/gT$ must be introduced as an electric (Debye) scale, whose influence appears as a Yukawa-type potential rather than a Coulomb-like one and $1/g^2T$ as a magnetic scale. In QCD, the magnetic mass, which cannot perturbatively be accessed, acts as a cut-off factor in the infrared problem and consequently becomes an essential element of thermal QCD.

The QCD coupling constant strength near the critical temperature T_c is still of the order of one. Therefore the perturbation theory is not applicable. However these regions are currently being investigated with great interest in many theoretical and experimental researches. After HTL (hard-thermal-loop) resummation was consistently formulated by Braaten and Pisarski, there were several improvements [7, 8] for unsolved problems. Comparison of this method with lattice numerical data has been reported; one-loop HTL calculations of free energy of QGP are in good agreement with the lattice numerical result [9, 10]. However, recent two-loop HTL calculation indicates that it does not yet have adequate convergence [11]. As another approach, 3-D reduction theory has also been widely studied and has yielded some promising arguments [12], but this method, which is defined only for the high temperature limit, cannot be applied to the confinement/deconfinement physics.

For reliable phenomenological analyses of high-energy heavy-ion collisions, it is important to obtain information on the magnetic and electric masses of gluons nonperturbatively; numerical study of lattice QCD as the first-principle calculation should play an important role here.

There have been many lattice studies of finite-temperature QCD, but only a few calculations of the electric and magnetic screening masses can be found in the literature [13], other than for the case of color $SU(2)$ [14, 15]. The electric mass has been estimated from the Polyakov loop correlation functions to obtain the screened heavy quark-antiquark potential [16, 17, 18].

The main aim of our study is to obtain reliable $SU(3)$ electric and magnetic masses through large-scale lattice QCD simulations and to reveal their temperature dependence [19]. We also compare our numerical data with the predictions of LOP (leading order perturbation), HTL resummation and other analyses.

Since our mass extraction is based on measuring a gauge dependent gluon propagator, it is important to check the gauge invariance of both screening masses [20]. This test is essential particularly for the magnetic mass because it has a poor definition in the frame of the perturbation.

Gluons are essential ingredients in QCD dynamics, and QCD undergoes phase transition from the confinement to the deconfinement phase when temperature increases. Therefore, we expect gluon propagators to show different behavior at each phase, and their study provides information on the confinement/deconfinement dynamics [21].

We measure gluon propagators which depend on the gauge used and therefore the gauge-fixing procedure is indispensable. However, gauge fixing on the lattice is difficult practically and conceptually. Usually, gauge fixing is carried out by the iterative technique [23], and it is very time consuming. The conceptual difficulty is that the gauge is not uniquely fixed; this is known as the Gribov copy problem [25]. In order to overcome these difficulties, we adopt here a stochastic quantization with Zwanziger's gauge-fixing term [26, 27, 28], instead of the path integral method.

In this paper, we extend our previous results on the $20^2 \times 32 \times 6$ lattice simulations [19] to the level which the present computer power can reach; we add more detailed values for the electric and magnetic masses and results at higher temperature from the larger lattice $32^2 \times 48 \times 6$ simulation. We also give detailed description of the algorithm employed in this study. In section 2, we describe the stochastic gauge quantization together with the Gribov copy problem. The definitions of the gluon propagator and electric and magnetic masses are given. A large part of section 3 is devoted to our simulation results on the small lattice $20^2 \times 32 \times 6$. First we describe all input parameters of the simulation and the statistics needed to measure reliable gluon propagators. Then we show the gluon behavior and the electric and magnetic masses extracted from it. The gauge dependence check and temperature dependence for both screening masses are also given. Finally we compare the numerical data with the perturbative argument and add the higher temperature result and remark about the finite volume effect. Section 4 gives the conclusions.

The main part of the calculation was carried out on the SX-5(NEC) vector-parallel computer of RCNP(CMC), Osaka Univ.. We used a parallel que with 4, 8 and 16 cpu and required about 6 months to complete this work.

II. STOCHASTIC GAUGE FIXING ON LATTICES AND GLUON PROPAGATORS

A. Lattice gauge action

The lattice regularization scheme of QCD is the gauge invariant Euclidean theory which enables us to perform the nonperturbative calculation based on the Monte Carlo numerical technique [29]. The simplest standard Wilson gauge action of lattice QCD can be defined from the continuum QCD as

$$S_g = \beta \sum (1 - \frac{1}{3} \text{Re} \text{Tr} [U_\nu(x) U_\mu(x + \hat{\nu}) U_\nu^\dagger(x + \hat{\mu}) U_\mu^\dagger(x)]), \quad \beta = \frac{2N_c}{g^2}. \quad (1)$$

Here, a link variable, $U_\mu(x)$, stands for the $SU(3)$ color gauge field:

$$U_\mu(x) = e^{iga_\mu A_\mu(x)}, \quad (2)$$

where a_μ is the lattice spacing, i.e, the lattice cut-off, and A_μ represents the gauge potential of the gluon. In this study, we adopt the quenched lattice simulation (pure gauge QCD) without a dynamical quark effect, using Eq.(1).

B. Gauge fixing and Gribov copy on lattices

We are interested in the direct calculation of the gluon propagator and the extraction of electric and magnetic screening masses from it. Therefore we must fix the gauge of gluon fields on the lattice, where the gauge transformation

is given by

$$U_\mu(x) \rightarrow \omega^\dagger(x)U_\mu(x)\omega(x + \hat{\mu}). \quad (3)$$

ω stands for a gauge rotation matrix $\in SU(3)$ on the lattice.

In this study, we focus on the Lorentz-type gauge, which is defined in the continuum as

$$\partial_\mu A_\mu(x) = 0, \quad (4)$$

while on the discrete lattice theory,

$$\Delta^a(x) \equiv \sum_{\mu=1}^4 2 \operatorname{Im} \operatorname{Tr} t^a \{U_\mu(x) - U_\mu(x - \hat{\mu})\} = 0. \quad (5)$$

Here, t^a is the $SU(N)$ generator with the relation $\operatorname{Tr}[t^a t^b] = \frac{1}{2}\delta^{ab}$. The above condition (5) is equivalent to

$$\begin{aligned} \delta_\omega I &= 0, \\ I &\equiv \sum_{x,\mu} \operatorname{Re} \operatorname{Tr} \omega^\dagger(x)U_\mu(x)\omega(x + \hat{\mu}). \end{aligned} \quad (6)$$

Wilson [22] and Mandula and Ogilvie [23] suggested the following condition for the gauge fixing method on the lattice:

$$\operatorname{Max.}_\omega I. \quad (7)$$

The continuum version of Eq.(7) was discussed in Refs. [30] and [31].

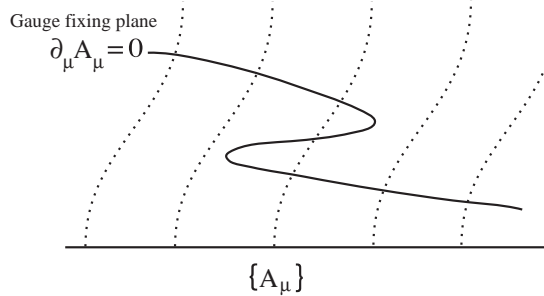


FIG. 1: Gribov [25] pointed out that a gauge is not uniquely fixed for non-Abelian theories, which is called the Gribov copy problem. This does not appear in the perturbative frame. The existence of the Gribov copy has been confirmed in several works [32, 33, 34].

The conditions (6) and (7) are not equivalent to each other since there may be local maxima or minima of I which satisfy Eq.(6). The gauge-fixing configuration cannot uniquely be fixed; this is called the “Gribov copy” [25] and is illustrated in Fig. 1. If we study this problem using the numerical lattice simulation based on the iterative procedure, it is very difficult to find a true maximum.

C. Stochastic gauge fixing

Our approach to the gauge-fixing procedure is to use the stochastic gauge quantization instead of the Monte Carlo path integral. The stochastic quantization is based on the Langevin equation that introduces virtual time in addition to the Euclidean coordinate. Zwanziger introduced a gauge-fixing term as

$$\frac{dA_\mu^a}{d\tau} = -\frac{\delta S}{\delta A_\mu^a} + \frac{1}{\alpha} D_\mu^{ab}(A) \partial_\nu A_\nu^b + \eta_\mu^a, \quad (8)$$

where $D_\mu^{ab}(A)$ is a covariant derivative, τ stands for Langevin time, and η is a Gaussian noise term. The second term on the r.h.s. is a gauge-fixing term. α is a gauge parameter; $\alpha = 0$ corresponds to the Lorentz gauge and $\alpha = 1$ to the Feynman gauge.

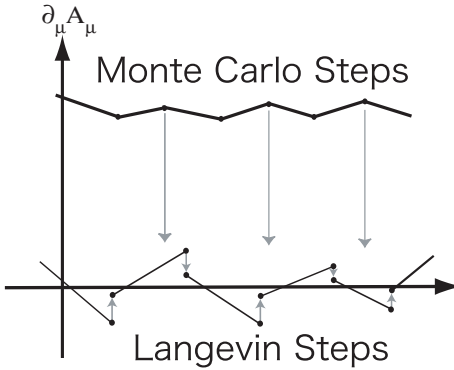


FIG. 2: The figure illustrates the gauge fixing procedure by the Wilson-Mandula-Ogilvie iterative method and stochastic gauge fixing. Gray arrow lines mean the gauge rotation for each algorithm. In the former algorithm, Monte Carlo update steps are performed without restriction on the $\partial_\mu A_\mu = 0$ plane. When a gauge fixed configuration is needed, the gauge configuration is rotated to the gauge-fixed plane, $\partial_\mu A_\mu = 0$, by iteration [23]. On the other hand, in the case of Langevin gauge fixing, configurations are updated by fluctuation around $\partial_\mu A_\mu = 0$.

Mizutani and Nakamura [28] developed the lattice version of the stochastic gauge fixing. The link variables are rotated through the following gauge transformation depending on the virtual time:

$$U_\mu(x, \tau + \Delta\tau) = \omega^\dagger(x, \tau) e^{if_\mu^a t^a} U_\mu(x, \tau) \omega(x + \hat{\mu}, \tau). \quad (9)$$

Here, f stands for the force,

$$f_\mu^a = -\frac{\partial S}{\partial A_\mu^a} \Delta\tau + \eta^a \sqrt{\Delta\tau}, \quad (10)$$

and the gauge rotation matrix is given by

$$\omega = e^{i\beta \Delta^a t^a \Delta\tau / \alpha}. \quad (11)$$

If $\omega = I$, Eq. (9) is lattice Langevin process. Gauge rotation, Eq. (9), with Eq. (11) leads to the gauge fixing term as $\Delta\tau \rightarrow 0$. Eq. (9) means the gauge rotation and Langevin step are executed alternately, as illustrated in Fig. 2.

In this stochastic quantization with Lorentz type gauge-fixing, Δ^a fluctuates around the gauge-fixing plane, $\Delta^a = 0$. For example, when we take $\alpha = 1.0$ and $\Delta\tau = 0.01$, Δ^a on $4^3 \times 8$ with $\beta = 6.0$ behaves as shown in Fig. 3. We confirm that Δ^a fluctuates around $\Delta^a = 0$ and gauge configurations are fixed on the $\partial_\mu A_\mu = 0$ plane enough.

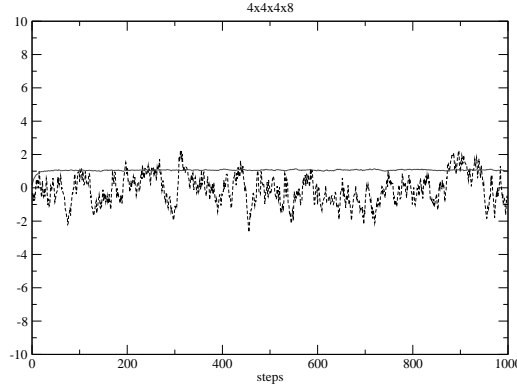


FIG. 3: These data are produced on the lattice $4^3 \times 8$ with $\Delta\tau = 0.01$ (Langevin step interval), $\alpha = 1.0$ (gauge parameter) at $\beta = 6.0$. The solid line means the average of $\sum_{x,a} \{\Delta^a(x)\}^2$, while the dashed line is the value of $\Delta^1(1)$. Δ^a fluctuates around $\Delta^a = 0$ and gauge configurations are fixed on the $\partial_\mu A_\mu = 0$ plane enough.

There are two reasons for using the stochastic gauge-fixing method in this study. One is a practical issue. When we use the standard Wilson-Mandula gauge-fixing method [23], the iterative procedure is applied to accepted gauge

configurations for each Monte Carlo step in Fig. 2. Then the number of iterations is unpredictable, particularly for large lattices. On the other hand, in algorithm (9), we simultaneously repeat the step of update and gauge rotation in Fig. 2 and are free from the convergence problem of gauge fixing. Therefore we can estimate precisely CPU time. Moreover, this algorithm, in which the gauge parameter α can be changed at will, is advantageous when testing gauge invariance.

A conceptual problem is the Gribov ambiguity [25]. The algorithm has a noteworthy feature, i.e., the second term of Eq. (8) gives rise to the configuration such that

$$\begin{aligned} \frac{d}{d\tau} \sum_x \Delta^2 &< 0 \text{ in } \Omega \\ &> 0 \text{ out of } \Omega. \end{aligned} \quad (12)$$

Here, Ω stands for the Gribov region,

$$\text{Gribov region : } \Omega \equiv \{A_\mu^a(x) | \partial_\mu A_\mu^a(x) = 0, -\partial_\mu D_\mu^{ab} > 0\}. \quad (13)$$

Namely, the stochastic gauge-fixing term is attractive (repulsive) inside (outside) the Gribov region [26, 27] if we start from the trivial configuration $\{A_\mu = 0\}$. Although our algorithm may not completely eliminate copies, we conclude that it is a more effective method.

Since the update algorithm described here is not so popular like the Metropolis or pseudo heatbath method, we show autocorrelation of the Polyakov loop.

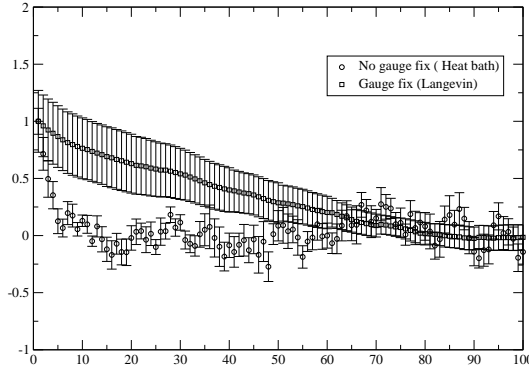


FIG. 4: Autocorrelation of the Polyakov loops for the Langevin with the stochastic gauge fixing ($\Delta\tau = 0.03$) and the pseudo-heat bath update algorithms as a function of the iteration steps. This calculation is done at $\beta = 6.1$ on the $8^3 \times 4$ lattice.

D. Definition of gluon propagators

We define the gauge field $A_\mu(x)$ in terms of the link variables as

$$A_\mu(x) = 2 \sum_a t^a \text{ImTr} t^a U_\mu(x). \quad (14)$$

We calculate massless gluon correlation functions with finite momentum,

$$G_{\mu\nu}(p_x, p_y, p_t, z) = \langle \text{Tr} A_\mu(p_x, p_y, p_t, z) A_\nu(-p_x, -p_y, -p_t, 0) \rangle. \quad (15)$$

In our study, to avoid the mixture of the longitudinal and transverse modes, we adopt the transverse conditions $p_i \cdot A_i = 0$ and measure the partially Fourier transformed propagator including one momentum $p_x = \frac{2\pi}{N_x}$ or $p_y = \frac{2\pi}{N_y}$ [32]. We will obtain the gluon mass using a lattice energy-momentum relation. This is the point different from other calculations [13, 14] where the mass extraction from zero momentum propagator was studied.

In the thermal perturbative QCD [2, 3, 4], the electric mass is defined from the temporal part of a gluon polarization tensor, $\Pi_{\mu\nu}$, while its spatial part is considered as the magnetic mass. Thus we can construct an electric propagator using a temporal one.

$$G_e(p, z) \sim \frac{1}{2} \left[G_{tt} \left(\frac{2\pi}{N_x}, 0, 0, z \right) + G_{tt} \left(0, \frac{2\pi}{N_y}, 0, z \right) \right]. \quad (16)$$

TABLE I: We estimate a lattice cut-off and its temperature scale by using mainly QCD_TARO fit function [36, 37]. We adopt $T_c \sim 256$ [35].

β	$a^{-1}[\text{GeV}]$	T[MeV]	T/T_c	β	$a^{-1}[\text{GeV}]$	T[MeV]	T/T_c
5.8	1.33	222	0.86	6.4	3.52	586	2.29
5.90	1.62	270	1.05	6.5	4.12	690	2.69
5.95	1.77	295	1.15	6.6	4.60	767	2.99
6.0	2.04	340	1.32	6.7	5.24	874	3.41
6.05	2.09	349	1.36	6.8	5.96	994	3.88
6.1	2.27	378	1.47	6.9	6.76	1128	4.40
6.2	2.64	447	1.74	7.0	7.64	1274	4.97
6.3	3.05	509	1.99	7.1	8.61	1436	5.61

In the same way, a magnetic propagator is defined by spatial components,

$$G_m(p, z) \sim \frac{1}{2} \left[G_{xx}(0, \frac{2\pi}{N_y}, 0, z) + G_{yy}(\frac{2\pi}{N_x}, 0, 0, z) \right]. \quad (17)$$

Because the screening mass is given as a pole of the denominator of the momentum space propagator, $1/(p^2 + m^2)$, $G_e(z)$ and $G_m(z)$ are expected to behave as exponential damping functions in the z direction on the distances, $Z \geq 1/T$ with the masses,

$$G_{e(m)}(z) \sim e^{-E_{e(m)}(p)z}. \quad (18)$$

III. RESULTS

A. Simulation parameters

We use mainly the lattice of the size $N_x N_y N_z N_t = 20^2 \times 32 \times 6$ which satisfies the condition $N_x \geq 3N_t$. On this lattice the long range area corresponds to $z \geq 1/T$ and then reliable information for screening physics may be produced.

We summarize lattice cut-off values and corresponding temperature in Table I. Varying the β , i.e., the lattice coupling constant, we change the temperature, $T = 1/N_t a$. The pure gauge lattice with $N_t = 6$ has critical $\beta_c \sim 5.89$ and we adopt $T_c \sim 256$ [35] as the critical temperature. To estimate the lattice cut-off value, we employ the results in Refs.[36, 37].

In addition, we prepare lattice of the size $32^2 \times 48 \times 6$ in order to investigate the finite size effect of screening masses, and to obtain them at higher temperature.

B. Necessary statistics to obtain reliable gluon propagators

We observe a large fluctuation of the gauge propagators, particularly at long distances, i.e., we suffer from long auto-correlation time. We show in Fig. 5 typical behavior of gluon propagators $G(z)$ as a function of the Langevin step. In order to analyse the gluon propagator and measure the screening masses we require $0.2 \sim 0.4$ million steps as the typical number of simulation data.

C. Gluon propagators

Although the gluon propagator itself is gauge dependent, it gives us some insights into the gluon dynamics about the confinement/deconfinement physics.

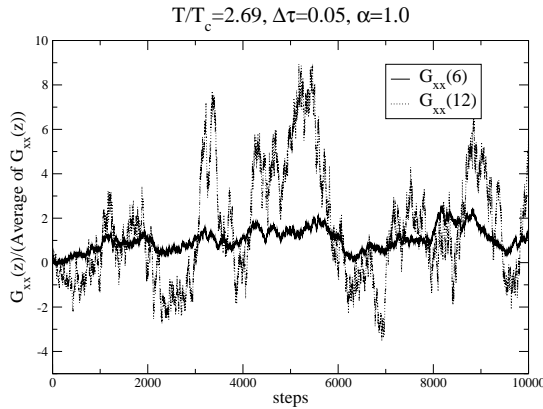


FIG. 5: Typical gluon propagator behavior as a function of Langevin steps on the lattice $20^2 \times 32 \times 6$. We find that fluctuations of $G_{xx}(12)$ are much larger than those of $G_{xx}(6)$. In order to investigate the screening effect, the long range contribution should be adopted. Consequently we need a large number of statistics.

The electric propagator is shown in Fig.6 [44], where the free massless propagator is also shown by dashed line. Gluons at short distances, i.e., $z < 6 = 1/T$, have very similar behavior to the free propagator. However, at long distances, gluon propagators decrease more rapidly than the free one. This indicates that the electric screening mass does not vanish at all temperatures.

Comparing data below and above T_c , we find the dynamics of the gluon is completely different in the confinement and deconfinement regions. The electric gluon mass in the confinement region becomes heavier; the electric gluon is completely screened in the confinement regions. This was first observed in Ref.[21]. Consequently, we cannot employ the assumption, Eq.(18). On the contrary, the propagator in the deconfinement regions decreases exponentially even at long distances with a finite mass.

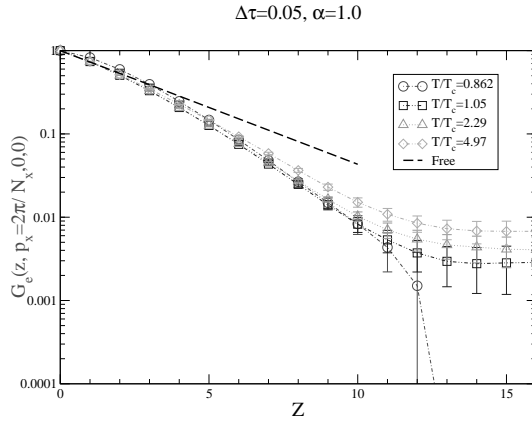


FIG. 6: The electric propagator in the confinement (circle) and deconfinement regions (the others) with $P_{x(y)} = \frac{2\pi}{N_x(y)}$. All propagators are found to become massive comparing with the free propagator (long dashed line). In the confinement regions, the propagator at long distances behaves like a very massive particle and vanishes, whereas the propagator beyond T_c has a finite mass.

Similar behavior is seen in the magnetic parts in Fig. 7; though the long distance magnetic gluons have large errors here, all magnetic gluons are found to be massive at long distances in the confinement/deconfinement phase and their effective mass in the confinement phase is heavier. We notice that the short distance behavior of magnetic gluons in the deconfinement regions looks unconventional. The magnetic gluon propagators draw a convex line at short distances while the electric ones do not so. The magnetic gluons behave as if they had an imaginary screening mass or negative spectral function which may tell the reason why the magnetic mass is not screened at least in LOP calculation.

As clearly seen in Fig. 7 and as we discussed below, the effective mass of the magnetic mass is z dependent. We take the value around $z = 1/T$ as electric case, since it is a relevant quantity at finite temperature screening.

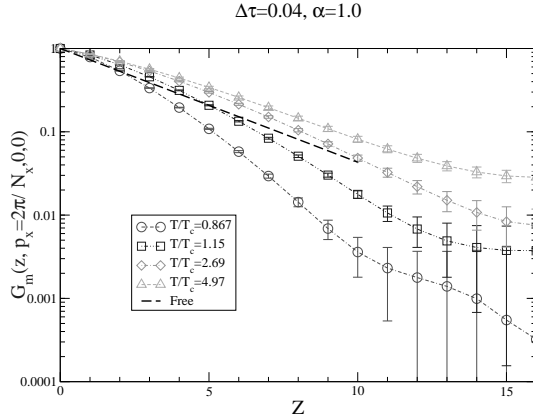


FIG. 7: The magnetic gluon propagator in the confinement (circle) and deconfinement regions (the others) with $P_{x(y)} = \frac{2\pi}{N_x(y)}$. Although the magnetic gluon propagators in this figure have large errors at long distances, they seem to have similar behavior to the electric part, except its short distance behavior in the deconfinement regions.

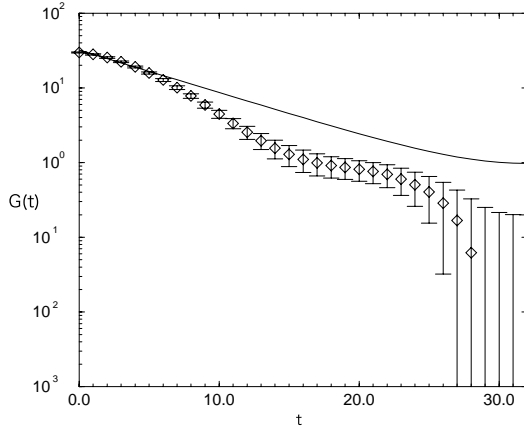


FIG. 8: Transverse gluon propagator, $G_T(t)$ with $\mathbf{p} = (\frac{2\pi}{N_x}, 0, 0)$, on $48^3 \times 64$ at $\beta = 6.8$ (confinement phase). Solid line represents the free propagator [21].

Gluons are essential ingredient of QCD but they are confined below T_c . As shown in Fig. 8, their propagator is convex upward at several regions. This is possible only when the spectral function is *not* positive definite. This peculiar behavior was first observed in Ref.[23], and confirmed in Ref.[24]. The feature does not contradict the fundamental postulate of quantum field theories, because gluons in the confinement region are not a physically observable particle. Instead, this is a glimpse of the confinement mechanism at infra-red regions which is still far from our understanding. Gribov's conjecture for gluon propagator,

$$G(p) \sim \frac{Z}{p^2 + \frac{b^4}{p^2}} \quad (19)$$

vanishes at $p^2 = 0$, and its Fourier transformation to the coordinate space is not convex downward, [45]

$$\tilde{G}(t) \sim \frac{Z}{r} e^{rt \cos \phi} \cos(rt \sin \phi + \phi) \quad (20)$$

where $r \equiv (|p|^4 + b^4)^{1/4}$ and $\phi \equiv \frac{1}{2} \tan^{-1} \frac{b^2}{p^2}$. The upward convex shape of the gluon propagators at the deconfinement region may provide us hints for glue dynamics.

Below the critical temperature T_c , we obtain similar result even for electric gluons at short distances. This seems natural since the perturbative argument in the confinement regions is generally not suitable and the confining correlation function would give also the negative spectral function.

D. Mass as a pole

To obtain the screening mass from the propagators, the following formula is used,

$$G_{e(m)} \sim \cosh(E_{e(m)}(p)(z - N_z/2)). \quad (21)$$

We employ data for $z \geq 1/T (= N_t a)$, because the screening effect occurs at sufficiently long distances. All fittings are almost done well from $z = 6$ to $N_z/2$, and $\chi^2/NDF \sim O(1)$.

To obtain the final result at $\Delta\tau = 0$, we must extrapolate data with respect to Langevin step width. The Runge-Kutta algorithm is applied to reduce the finite Langevin step $\Delta\tau$ dependence [38]. We perform simulations for a set of parameters with $\Delta\tau = 0.03 \sim 0.05$. Table IV and Fig. 9 represent $E(p)$ measured here versus $\Delta\tau$. The slight dependence of $\Delta\tau$ enables us to use a linear function when fitting data. We finally obtain the mass from $E(p)$ by the

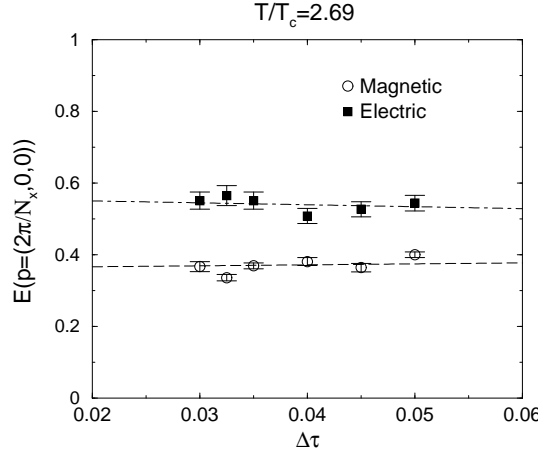


FIG. 9: $\Delta\tau$ dependence of masses is slight. Finally to obtain a final value at $\Delta\tau = 0$, we use the linear function for the extrapolation.

following lattice energy-momentum relation [14] [46] ,

$$\sinh^2 \frac{Ea}{2} = \sinh^2 \frac{ma}{2} + \sum_{i=1}^3 \sin^2 \frac{p_i a}{2}. \quad (22)$$

TABLE II: This shows the typical example of the Langevin step dependence at $T/T_c = 2.69$. For all simulations for $\Delta\tau = 0.03 \sim 0.05$, approximately $0.2 \sim 0.4$ million steps (measurements) are used after eliminating about $3 \sim 5$ thousand steps as thermalization. “ $\mathbf{p} \neq 0$ ” means including the momentum $P_{x(y)} = 2\pi/N_{x(y)}$. We extrapolate these data to $\Delta\tau = 0$, and then obtain $m_{ea}(p_\mu = 0) = 0.470(38)$ and $m_{ma}(p_\mu = 0) = 0.199(52)$ using lattice energy-momentum relation.

$\Delta\tau$	Number of steps	$m_{ma}(\mathbf{p} \neq 0)$	$m_{ea}(\mathbf{p} \neq 0)$
0.05	275000	0.400(08)	0.544(22)
0.045	240000	0.364(12)	0.527(21)
0.04	380000	0.381(11)	0.508(21)
0.035	280000	0.369(08)	0.551(24)
0.0325	300000	0.336(09)	0.565(28)
0.03	320000	0.367(14)	0.551(24)
0.00		0.369(46)	0.561(40)

TABLE III: Temperature dependence of the electric and magnetic masses which are extrapolated to the Langevin step $\Delta\tau = 0$.

T/T_c	m_e/T	m_m/T	T/T_c	m_e/T	m_m/T
1.05	1.506(438)	2.802(054)	2.69	2.820(228)	1.194(312)
1.15	2.694(288)	2.484(258)	2.99	2.892(234)	1.590(318)
1.32	3.348(408)	2.406(246)	3.41	2.190(450)	0.960(168)
1.36	2.904(336)	1.986(296)	3.88	2.292(222)	0.852(318)
1.47	3.138(342)	1.866(222)	4.40	2.598(168)	1.134(414)
1.74	2.700(426)	1.620(300)	4.97	2.310(084)	0.804(638)
1.99	2.898(498)	1.608(270)	5.61	2.106(390)	0.486(336)
2.29	2.484(234)	0.990(264)			

E. Gauge invariance

The screening mass is physical and expected to be gauge invariant. However, since the gluon propagator defined by Eq.(16) and (17), are gauge dependent, it is important to check whether the screening masses obtained here are gauge invariant or not. In addition, since the magnetic mass can not be defined by the perturbative calculation, it is particularly important to check its gauge dependence. In Fig. 10, we show the gauge parameter α dependence of electric and magnetic masses. Gauge dependence of both screening masses is found to be very slight, namely the result strongly suggests that they are gauge invariant and physical observables.

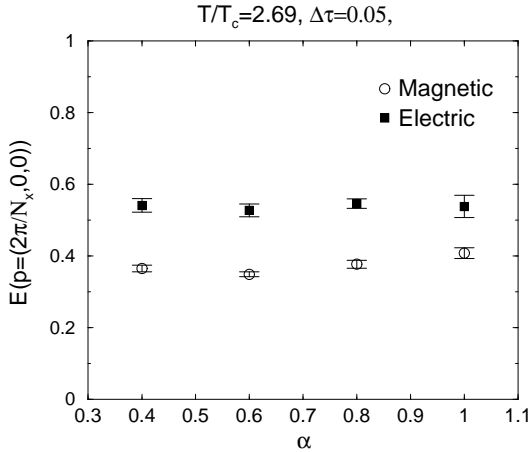


FIG. 10: Gauge dependence for electric and magnetic screening masses. Gauge dependence of both screening masses is very slight.

F. Temperature dependence

We study the temperature dependence of the screening mass in the range, $T/T_c = 1 \sim 6$ which would be realized in high-energy heavy ion collision experiments such as RHIC or LHC [40]. Table III and Fig. 11 show electric and magnetic masses as a function of the temperature. The magnetic part definitely has nonzero mass in this temperature region. As T increases, both $m_{e(m)}/T$ decrease monotonically, and at almost all temperatures, the magnetic mass is less than the electric one, except very near T_c where the electric mass decreases very quickly as T approaches T_c .

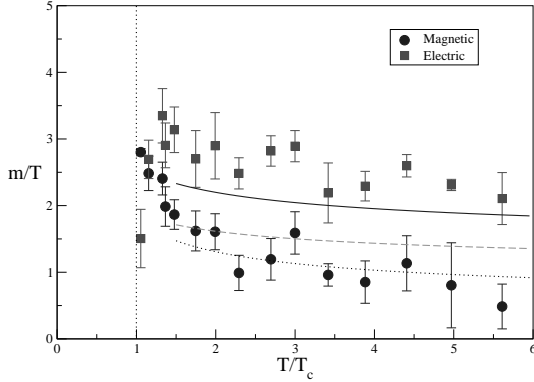


FIG. 11: Temperature dependence of electric and magnetic screening masses. The dotted line is fitted by the assumption, $m_g \sim g^2 T$. For the electric mass, the dashed and solid lines represent LOP and HTL resummation results, respectively.

G. Comparison with LOP and HTL resummation results

We perform a fitting analysis for our numerical results using the following ansatz,

$$\frac{m_e}{T} = C_e g(T), \quad \frac{m_m}{T} = C_m g^2(T), \quad (23)$$

whose g -dependence is predicted by the perturbative and 3-D reduction analysis [3, 4] and we assume C_e and C_m are free parameters. In the following discussion, the data above $T \sim 1.5T_c$ are used. Here, we use the running couplings as

$$g^2(\mu) = \frac{1}{2b_0 \log(\mu/\Lambda)} \left(1 - \frac{b_1}{2b_0} \frac{\log(2 \log \mu/\Lambda)}{\log(\mu/\Lambda)} \right), \quad (24)$$

and we set $\mu = 2\pi T$ which is Matsubara frequency as the renormalization point and $\Lambda = 1.03T_c$ [9] as QCD mass scale. b_0 and b_1 are the first two universal coefficients of the renormalization group,

$$b_0 = 11N_c/48\pi^2, \quad b_1 = (34/3)(N_c/(16\pi^2))^2. \quad (25)$$

As a result, we obtain

$$\begin{aligned} C_e &= 1.63(3), & \chi^2/\text{NDF} &= 0.715, \\ C_m &= 0.482(31), & \chi^2/\text{NDF} &= 0.979. \end{aligned} \quad (26)$$

The scalings expected in Eq.(23) for electric and magnetic masses are found to work well. However, the magnitude of C_e is larger than $C_e^{\text{LOP}} = 1$. On the other hand, for magnetic mass, a self-consistent inclusion technique in Ref. [39] gives $m_g = 0.568g^2 T$ that is close to our fitting result.

The HTL resummation technique applying the free energy of hot gluon plasma has been widely discussed [9, 10]. Rebhan gave a formula for the electric mass in the one-loop HTL perturbation theory [41] and for the case of $SU(3)$,

$$m_e^2 = m_{e,0}^2 \left[1 + \frac{3g}{2\pi} \frac{m_e}{m_{e,0}} \left(\log \frac{2m_e}{m_m} - \frac{1}{2} \right) + O(g^2) \right], \quad m_{e,0} = gT. \quad (27)$$

Here, we assume the magnetic mass to be of the order of g^2 . Substituting our fitted value for m_m , we can iteratively solve the above equation. In Fig. 11, we show this HTL resummation together with LOP result. The HTL result gives a better description than the naive perturbation, upon comparing our numerical experiment.

The electric mass was obtained also by a heavy $q\bar{q}$ potential from $SU(3)$ Polyakov loop correlator at finite temperature in Refs. [17, 18]. Our results here are inconsistent with theirs, since the mass extraction from the heavy $q\bar{q}$ potential cannot consistently be performed due to ambiguity of its fitting assumption. Besides, 3-D reduction argument [12] has shown that m_e/gT goes down when T increases, but even at $T \sim 1000\Lambda_{\overline{MS}}$ the electric mass is still about $3m_{e,0}$. This observation agrees qualitatively with our analysis.

TABLE IV: Data extracted from the small and large lattices at the same coupling regions, $\beta = 7.5$ and $\beta = 8.0$.

β	$\Delta\tau$	$m_{ma}(\mathbf{p} \neq 0)$	$m_{ea}(\mathbf{p} \neq 0)$
small lattice size $20^2 \times 32 \times 6$			
7.5	0.05	0.301(15)	0.455(09)
8.0	0.04	0.311(09)	0.457(14)
large lattice size $32^2 \times 48 \times 6$			
7.5	0.05	0.231(03)	0.433(08)
8.0	0.04	0.214(04)	0.406(14)

H. Higher T and finite size effect

Although the main result in this paper is based on studies for the small lattice size $20^2 \times 32 \times 6$ as discussed in the previous section, we additionally perform the simulation on the large lattice $32^2 \times 48 \times 6$ to go to higher temperature regions and to check the finite size effect of the screening masses. However, as the lattice size increases, the behavior of the long distance gluon cannot be controlled because of a large fluctuation. The typical result on the large lattice is shown in Fig. 12. Even after the $0.3 \sim 0.4$ million measurements, we could not determine the electric gluon propagator at long distances ($z \geq 16$) while the magnetic gluon is properly correlated.[47] Nevertheless, provided that we adopt only the data of the intermediate regions above $z = 6$ until the disappearance of the propagator, we obtain similar results for the electric and magnetic masses as seen in Fig. 12 at the same temperature regions.

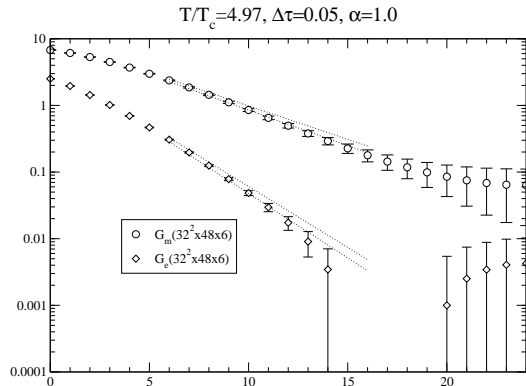


FIG. 12: Typical electric and magnetic propagators on the large lattice $32^2 \times 48 \times 6$ (opened), and the data for $20^2 \times 32 \times 6$ (dotted band line with error) are reproduced by using the values in Table III. Both calculations give very similar value for electric and magnetic parts.

Using the criterion describing above, we may consistently obtain both screening masses on the large lattice, and can argue that the magnetic mass has a stronger finite size effect than the electric one. $E(p)$ appeared in Eq.(17) are shown in the Table IV at $T/T_c = 8.99$ and 16.12 . The momenta for the small and large lattice are $p_x = 2\pi/N_x \sim 0.314$ and $p_x = 2\pi/N_x \sim 0.196$, respectively. Namely, the result on the small lattice implies the magnetic mass at high temperature ($T/T_c > 5$) seems to be going to zero, while on the large lattice it remains finite. [48]

Although it is very difficult to measure the long distance gluon propagators, we can add the higher temperature results ($T/T_c = 8.99, 16.12$) summarized in Table V. In Fig. 13 we again fit the data including these new points. The fit for the large lattice data by Eq. (23) hence results in

$$\begin{aligned} C_e &= 1.69(4), & \chi^2/NDF &= 0.66 \\ C_m &= 0.549(16), & \chi^2/NDF &= 1.27 \end{aligned} \quad (28)$$

These results are shown in Fig. 13. It should be noticed that C_e is the same value as given in Eq. (26), while $C_m \sim 10\%$ larger on the large lattice and is very close to $m_g = 0.568g^2T$ calculated by the self-consistent inclusion technique in Ref. [39].

TABLE V: Simulation parameters and the screening masses for the large lattice $32^2 \times 48 \times 6$. Lattice scales are estimated by Refs.[36, 37].

β	$a^{-1}[\text{GeV}]$	$T[\text{MeV}]$	T/T_c	m_m/T	m_e/T
7.0	7.64	1274	4.97	1.128(78)	2.556(156)
7.5	13.8	2303	8.99	1.014(54)	2.178(144)
8.0	24.7	4127	16.12	0.984(60)	2.256(120)

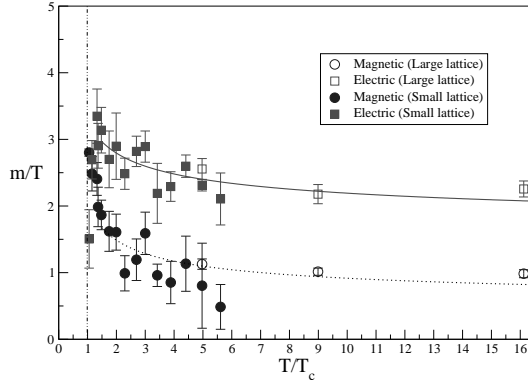


FIG. 13: The temperature dependence including higher temperature points on the large lattice $32^2 \times 48 \times 6$.

IV. CONCLUSIONS

We have measured the gluon propagators and obtained the electric and magnetic masses by lattice QCD simulations in the quenched approximation for $SU(3)$ between $T = T_c$ and $6T_c$. Features of QGP in this temperature region will be extensively studied theoretically and experimentally in near future.

Our screening mass studies are the first reliable measurement in $SU(3)$ lattice calculation. We mainly investigate the temperature dependence for electric and magnetic masses which do not vanish on $20^2 \times 32 \times 6$ lattices. At all temperature region we find the electric mass, m_e , is always larger than magnetic one, m_m , except near critical temperature point. As the temperature goes down T_c , m_e/T drops down quickly, while m_m/T is still going up. Consequently, using data above $T/T_c \sim 1.5$ we conclude the scalings, $m_e \sim gT$ and $m_m \sim g^2T$ work well. Furthermore, HTL resummation calculation has recently been developed and compared with nonperturbative lattice simulations. We also have compared our numerical results with LOP and HTL resummation and find the good improvement of HTL electric mass. These comparison studies of $SU(3)$ screening masses qualitatively seem to agree with the case of $SU(2)$ [14].

The electric masses obtained here are not consistent with those by a heavy $q\bar{q}$ potential calculations from $SU(3)$ Polyakov loop correlator at finite temperature in Refs. [17, 18]. In Ref.[18], the authors have done an extensive analyses with three different temporal extents and two different gauge actions, obtained very reliable potential as a function of the temperature. They observe that the potential above T_c can not be described properly by the leading order perturbation calculation up to a few T_c : They exclude the two gluon exchange as the dominant screening mechanism, and suggest that some kind of one-gluon exchange may describe the potential effectively as a result of the complex interaction, and that about 1.5 to 3 times T_c a mixture of one- and two-gluon exchange may explain the behavior. Therefore, due to the ambiguity of fitting assumption, it is not clear whether we can compare our screening masses directly with those by the potential calculation.

In order to investigate the nature of QGP, especially the excitation modes in the plasma, Datta and Gupta have recently calculated glueball masses at finite temperature and made an interesting observation. They measured screening masses of A_1^{++} (scalar) and A_2^{--} glueball, which allow two- and three- gluon exchange, and their ratio ~ 1.7 is near $3/2$. The A_2^{--} mass is twice of those obtained by Kaczmarek et al, and shows similar temperature dependence. There are now several non-perturbative methods to study QGP: our direct measurement of the gluon propagators,

glueball screening masses and the Polyakov line correlators. These analyses strongly suggest that QGP above T_c is far from free gas and has non-trivial structure. Much more detailed analyses in future are highly desirable.

The screening mass on the lattice is extracted from the gauge dependent propagator, and the magnetic mass is not well defined in perturbation theory. We have nonperturbatively confirmed the gauge invariance of both screening masses. In Ref. [20] it was reported that the $SU(2)$ magnetic propagator exhibits a complicated gauge dependent structure at low momentum. Therefore, since the gauge dependence for the screening masses is investigated within the Lorentz-type gauge fixing based on the stochastic gauge quantization in this study, we plan to extend our analysis to a simulation with Coulomb-type gauge fixing.

We have seen the qualitative difference of the gluon dynamics between the confinement and deconfinement phase by the direct propagator measurement. The electric and magnetic gluons in the confinement phase indicate a very massive particle behavior, while after the phase transition, they have a finite mass. In addition, in the deconfinement phase, the magnetic gluon at short distances seems to be still in the confinement phase. This may be related to the difficulty of the perturbative argument for spatial gluon components and the fact that magnetic Wilson loop gives non-zero spatial string tension even at high temperatures [43].

Magnetic mass has been a subject of many discussions. Perturbatively it is difficult to handle. To our knowledge, there is no complete perturbative calculation which is free from any assumption or model. Naive expectation is that it vanishes, but it is necessary to have a finite value as a cut-off factor in the infrared regime. On the other hand the finite spatial string tension even at $T > T_c$ indicates ‘confinement’ in the magnetic sector.

Our screening gluon magnetic propagators show indeed non-trivial behavior. At very short distance it may be consistent with massless behavior, but at finite distance we can not fit them by simple ansatz. It is distance dependent. The confinement is a property of long range, and the propagators there drop. Therefore it is a very interesting task in future to investigate the magnetic propagators at very long distance.

We calculated the gluon propagators on the larger lattice $32^2 \times 48 \times 6$ and observed the large error and strange behavior at long distances. Nevertheless, screening masses have been estimated and we find the magnetic mass is sensitive to the lattice size effect. Thus on too small lattice we can not deal with the magnetic mass consistently. Moreover, the simulation even at higher temperature $T/T_c \sim 9$ and 16 shows that nonperturbative results are far from LOP. This observation is compatible with that of Ref. [12, 14].

For the quantization with gauge fixing, the stochastic gauge fixing has been adopted. We think the stochastic gauge fixing has the better features to reduce some difficulties of a nonperturbative gauge fixing. It is consequently possible to do a practical simulation of gluon screenings effectively. However, we also see that the gluon propagators have large fluctuations and unexpected behavior at long distances and may need further devices.

The color screening data we obtained here are useful information for QGP phenomenology, for instance, jet quenching or heavy quark potential. We plan to study $q\bar{q}$ as well as qq potential relating a baryon bound state, nonperturbative QCD vertex calculation, quark propagators, etc. using the stochastic gauge fixing, which will help us to understand QGP.

V. ACKNOWLEDGEMENT

We would like to thank A. Niégawa, S. Muroya, T. Inagaki and I. Pushkina for many helpful discussions. The calculation was done on SX-5(NEC) vector-parallel computer. We really appreciate warm hospitality and much support of the RCNP administrators. HPC computer at INSAM, Hiroshima Univ is used also. This work is supported by Grant-in-Aide for Scientific Research by Monbu-Kagaku-sho (No.11440080, No. 12554008 and No. 13135216)

- [1] X.N. Wang, Phys. Lett. B **485**, 157 (2000).
- [2] D.J. Gross, R.D. Pisarski and L.G. Yaffe, Rev. Mod. Phys. **53**, 43 (1981).
- [3] J.I. Kapusta, *Finite-Temperature Field Theory* (Cambridge monographs on mathematical physics, Cambridge University Press, Cambridge, 1989).
- [4] M. Le Bellac, *Thermal Field Theory* (Cambridge monographs on mathematical physics, Cambridge University Press, Cambridge, 1996).
- [5] T. Muta, *FUNDATION OF QUANTUM CHROMODYNAMICS 2ND EDITION* (World Scientific Lecture Notes in Physics - Vol. 57 World Scientific Publishing Co. Pte. Ltd., 1998).
- [6] A.D. Lindé, Phys. Lett. B **96**, 289 (1980).
- [7] R.D. Pisarski, Phys. Rev. Lett. **63**, 1129 (1989); E. Braaten and R.D. Pisarski, Phys. Rev. Lett. **64**, 1338 (1990); E. Braaten and R.D. Pisarski, Nucl. Phys. **B337**, 569 (1990).

- [8] A. Niégawa, Phys. Rev. Lett. **73**, 2023 (1994).
- [9] J.O. Andersen, E. Braaten and M. Strickland, Phys. Rev. Lett. **83**, 2139 (1999).
- [10] J.-P. Blaizot, E. Iancu and A. Rebhan, Phys. Rev. Lett. **83**, 2906 (1999); Phys. Lett. **B470**, 181 (1999); Phys. Rev. D **63**, 065003 (2001).
- [11] J.O. Andersen, E. Braaten, E. Petitgirard and M. Strickland, Phys. Rev. D **66**, 085016 (2002).
- [12] K. Kajantie, M. Laine, J. Peisa, A. Rajantie, K. Rummukainen and M. Shaposhnikov, Nucl. Phys. B(Proc. Suppl.) **63** A-C, 418 (1998); Phys. Rev. Lett. **79**, 3130 (1997).
- [13] J.E. Mandula and M. Ogilvie, Phys. Lett. B **201**, 117 (1988).
- [14] U.M. Heller, F. Karsch and J. Rank, Phys. Lett. B **355**, 511 (1995); Phys. Rev. D **57**, 1438 (1998).
- [15] A. Cucchieri, F. Karsch and P. Petreczky, Phys. Lett. B **497** 80 (2001).
- [16] A. Irbäck, P. Lacock, D. Miller, B. Petersson and T. Reisz, Nucl. Phys. B **363**, 34 (1991).
- [17] M. Gao, Phys. Rev. D **41**, 626 (1990).
- [18] O. Kaczmarek, F. Karsch, E. Laermann and M. Lütgemeier, Phys. Rev. D **62**, 034021 (2000).
- [19] A. Nakamura, I. Pushkina, T. Saito and S. Sakai, Phys. Lett. B, **549**, 133(2002).
- [20] A. Cucchieri, F. Karsch and P. Petreczky, Phys. Rev. D **64** 036001 (2001).
- [21] A. Nakamura, Prog. Theor. Phys. Suppl. No. **131**, 585, 1998.
- [22] K.G. Wilson, in *Recent Developments in Gauge Theories*, ed. G. t'Hooft (Plenum Press, New York, 1980), 363.
- [23] J.E. Mandula and M. Ogilvie B **185**, 127 (1987).
- [24] H.Aiso, M.Fukuda, T.Iwamiya, M.Mizutani, A.Nakamura, T.Nakamura and M.Yoshida, Nucl.Phys. B (Proc. Suppl.) **42**, 1995, 899; H.Aiso, M.Fukuda, T.Iwamiya, A.Nakamura, T.Nakamura and M.Yoshida Prog. Theor. Physics, Suppl. No.122, 1996, 123.
- [25] V.N. Gribov, Nucl. Phys. **B139**, 1 (1978); *Gribov Theory of Quark Confinement*, Ed. by J. Nyiri, (World Scientific, Singapore, 2001).
- [26] D. Zwanziger, Nucl. Phys. **B192**, 259 (1981).
- [27] E. Seiler, I.O. Stamatescu and D. Zwanziger, Nucl. Phys. **B239**, 177 (1984).
- [28] A. Nakamura and M. Mizutani, *Vistas in Astronomy* (Pergamon Press), vol. **37**, 305 (1993); M. Mizutani and A. Nakamura, Nucl. Phys. B(Proc. Suppl.) **34**, 253 (1994).
- [29] K.G. Wilson Phys. Rev. D **10** , 2445 (1974).
- [30] T. Maskawa and H. Nakajima, Prog. Theor. Phys. **63** 641 (1980).
- [31] Semenov-Tyan-Shanskii and Franke, Zapiski Nauchnykh Seminarov, Leningradskage Otdeleniya Mathemat. Instituta im Steklov ANSSSR Vol. **120**, 159 (1982).
- [32] A. Nakamura and M. Plewnia, Phys. Lett. B **255**, 274 (1991).
- [33] S. Hioki, S. Kitahara, Y. Matsubara, O. Miyamura, S. Ohno and T. Suzuki, Phys. Lett. B **271**, 201 (1991).
- [34] V.G. Bornyakov, V.K. Mitrjushkin, M. Muller-Preussker and F. Pahl, Phys. Lett. B **317**, 596 (1993).
- [35] G. Boyd, J. Engels, F. Karsch, E. Laermann, C. Legeland, M. Lütgemeier and B. Petersson, Phys. Rev. Lett. **75**, 4169 (1995).
- [36] QCDSR collaboration, K. Akemi, et al., Phys. Rev. Lett. **71**, 3063 (1993).
- [37] C.R. Allton, hep-lat/9610016 (1996).
- [38] A. Ukawa and M. Fukugita, Phys. Rev. Lett. **55**, 1854 (1985); G.G. Batrouni, G.R. Katz, A.S. Kronfeld, G.P. Lepage, B. Svetitsky and K.G. Wilson, Phys. Rev. D **32**, 2736 (1985).
- [39] G. Alexanian and V.P. Nair, Phys. Lett. B **352**, 435 (1995).
- [40] B. Müller, Nucl. Phys. A **630** , 461c, (1998).
- [41] A.K. Rebhan, Phys. Rev. D **48**, R3967 (1993); Nucl. Phys. **B430**, 319 (1994).
- [42] S. Datta and S. Gupta, Phys. Rev. D **67**, 054503 (2003).
- [43] G. S. Bali, J. Fingberg, U. M. Heller, F. Karsch, and K. Schilling, Phys. Rev. Lett. **71**, 3059(1993).
- [44] In the following, all the propagators are normalized at $z = 0$, namely they are divided by $G_{e(m)}(z = 0)$ to compare each other.
- [45] We thank E. Seiler and D. Zwanziger for helpful discussions on this point.
- [46] We ‘assume’ this relation to extract the mass.
- [47] Magnetic propagator determination is also difficult near T_c .
- [48] Note that the data of $\beta = 7.5$ and 8.0 for the small lattice are considered to be preparative and we do not indeed use these data for our main studies by the previous section.